JACS
JOURNAL OF THE AMERICAN CHEMICAL SOCIETY

ARTICLE

pubs.acs.org/JACS

# Mechanistic and Physiological Implications of the Interplay among Iron−Sulfur Clusters in [FeFe]-Hydrogenases. A QM/MM Perspective

Claudio Greco,*[,†,‡] Maurizio Bruschi,[§] Piercarlo Fantucci,[†] Ulf Ryde,[⊥] and Luca De Gioia*[,†]

[†]Department of Biotechnology and Bioscience, University of Milan-Bicocca, Piazza della Scienza 2, 20126, Milan, Italy
[‡]Department of Chemistry, Humboldt-Universitaet zu Berlin, Brook-Taylor-Strasse 2, 12489, Berlin, Germany
[§]Department of Environmental Sciences, University of Milan-Bicocca, Piazza della Scienza 1, 20126, Milan, Italy
[⊥]Department of Theoretical Chemistry, Lund University, P.O. Box 124, 22100 Lund, Sweden

Supporting Information

**ABSTRACT:** Key stereoelectronic properties of *Desulfovibrio desulfuricans* [FeFe]-hydrogenase (DdH) were investigated by quantum mechanical description of its complete inorganic core, which includes a $Fe_6S_6$ active site (the H-cluster), as well as two ancillary $Fe_4S_4$ assemblies (the F and F′ clusters). The partially oxidized, active-ready form of DdH is able to efficiently bind dihydrogen, thus starting $H_2$ oxidation catalysis. The calculations allow us to unambiguously assign a mixed Fe(II)Fe(I) state to the catalytic core of the active-ready enzyme and show that $H_2$ uptake exerts subtle, yet crucial influences on the redox properties of DdH. In fact, $H_2$ binding can promote electron transfer from the H-cluster to the solvent-exposed F′-cluster, thanks to a 50% decrease of the energy gap between the HOMO (that is localized on the H-cluster) and the LUMO (which is centered on the F′-cluster). Our results also indicate that the binding of the redox partners of DdH in proximity of its F′-cluster can trigger one-electron oxidation of the $H_2$-bound enzyme, a process that is expected to have an important role in $H_2$ activation. Our findings are analyzed not only from a mechanistic perspective, but also in consideration of the physiological role of DdH. In fact, this enzyme is known to be able to catalyze both the oxidation and the evolution of $H_2$, depending on the cellular metabolic requirements. Hints for the design of targeted mutations that could lead to the enhancement of the oxidizing properties of DdH are proposed and discussed.

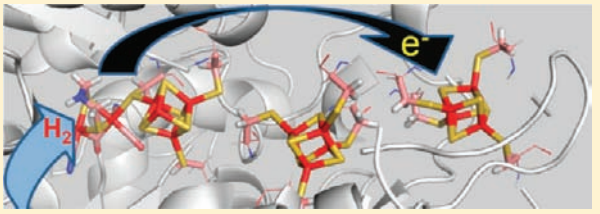


## INTRODUCTION

[FeFe]-hydrogenases are iron-containing enzymes that efficiently catalyze the reversible oxidation of $H_2$. The chemistry of this enzyme class depends on the unique features of an organometallic cofactor, the H-cluster (Figure 1). The latter is composed of two subclusters covalently linked to each other by the sulfur atom of a cysteine residue,[1] viz., an $Fe_4S_4$ subcluster, named $[4Fe-4S]_H$ in the following text, and an $Fe_2S_2$ assembly directly involved in substrate binding. The latter subcluster is usually termed $[2Fe]_H$ and it includes biologically unusual ligands, viz., three carbonyls (one of which in a (semi)bridging position),[1b,2] two cyanides, and a dithiolate ligand that, according to recent spectroscopic,[3] biochemical[4] and theoretical[3b,5] investigations, should be a di(thiomethyl)amine (DTMA) residue.

The Mössbauer,[6] electron paramagnetic resonance (EPR),[7] and electron−nuclear double resonance[8] (ENDOR) properties of the [FeFe]-hydrogenases characterized up to now are largely superimposable[9] and highlight a complex redox chemistry, owing to the presence of ancillary iron−sulfur clusters that flank the H-cluster in most of the known [FeFe]-hydrogenases. The conservation of the amino acids in the vicinity of the cofactors suggests that the redox properties of the metal clusters are finely tuned to control [FeFe]-hydrogenase function. For example, the reversibility of dihydrogen oxidation catalysis is thought to depend on a tight balance of the redox potential of the catalytic and ancillary clusters.[10,11] However, only few details are known about the interplay between the H-cluster and the other Fe−S clusters in [FeFe]-hydrogenases.

The [FeFe]-hydrogenases from *Desulfovibrio desulfuricans* (DdH) and *D. vulgaris* Hildenborough (DvH), which share the same amino acid sequence,[7a,12,13] have undergone extensive characterization,[9,10] and the structure of DdH has also been resolved by X-ray spectroscopy.[1a] In addition, DdH includes not only the H-cluster but also two classical ferredoxin-like $Fe_4S_4$ clusters, which in the following will be referred to as the accessory F and F′ clusters (Figure 2).

Differently from several [FeFe]-hydrogenases variants that are irreversibly inactivated when purified in aerobic and nonreducing conditions (e.g., the two [FeFe]-hydrogenases expressed by *Clostridium pasteurianum*, CpI and CpII), DdH and DvH can be activated after aerobic purification.[10] The aerobically purified enzyme ($DH_{oxair}$ in the following) is overoxidized and inactive. EPR measurements have shown that $DH_{oxair}$ is diamagnetic, which implies that all the $Fe_4S_4$ assemblies (i.e., the $[4Fe-4S]_H$, F, and F′ moieties) are in the oxidized, 2Fe(II)2Fe(III) state.[9]

**Received:** June 15, 2011
**Published:** September 26, 2011





dx.doi.org/10.1021/ja205542k | *J. Am. Chem. Soc.* 2011, 133, 18742–18749

However, reductive titration experiments at temperatures lower than 80 K showed that $DH_{oxair}$ can be converted into an EPR-active form. In particular, the intensity of the EPR signal was reported to reach its maximum at −110 mV and starts declining at potentials more negative than −200 mV.[14] Concomitantly with the decrease of the first EPR signal, another EPR signal appears, which was shown to dominate the EPR spectrum at potentials around −250 mV.[14] Both signals were ascribed to the catalytic H-cluster, more specifically to a transient enzyme state ($DH_{trans}$) in which the $[4Fe-4S]_H$ subcluster is reduced to the 3Fe(II)Fe-(III) state, and to the active-ready form of the enzyme ($DH_{ox}$), in which the $[2Fe]_H$ subcluster has become paramagnetic as a result of a one-electron reduction at the expense of the $[4Fe-4S]_H$ subcluster.[15] Such electron transfer within the H-cluster in the $DH_{trans}/DH_{ox}$ transition was proposed to be triggered by an H-cluster conformational rearrangement, the details of which are presently unknown.[9,15] However, it has been also proposed that the $DH_{trans}/DH_{ox}$ conversion implies two-electron reduction.[16]

In $DH_{ox}$ the accessory F and F′ clusters attain the diamagnetic 2Fe(II)2Fe(III) redox state. In fact, no signals assignable to the F and F′ clusters could be detected in the enzyme EPR spectrum at potentials less negative than −250 mV.[14] The EPR signal of $DH_{ox}$ reaches the maximum intensity at −300 mV, but at −320 mV it suddenly disappears, while the concomitant development of a complex EPR signal is observed, the latter featuring a midpoint potential of −305 mV. This complex EPR signal was attributed to the completely reduced enzyme ($DH_{red}$), featuring an EPR-silent H-cluster and EPR-active F and F′ clusters in the reduced 3Fe(II)Fe(III) state.[7,14]

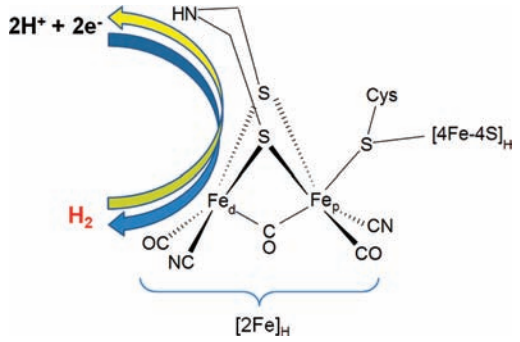


**Figure 1.** Structural features of the H-cluster: the [FeFe]-hydrogenase active site, directly involved in $H_2$ evolution and oxidation.

While states such as $DH_{oxair}$ and $DH_{trans}$ are not observed in all known [FeFe]-hydrogenases because the reductive activation is relevant only for enzymes that can be purified aerobically, the partially oxidized $DH_{ox}$ state has counterparts in all [FeFe]-hydrogenases that have been studied by EPR.[9,10] In fact, the $DH_{ox}$ state of the enzyme, together with the $DH_{red}$ state, play a crucial role in catalysis.[9] However, while $DH_{red}$ is thought to correspond to a mixture of different protonation states of the enzyme[17] and its detailed structural features are still matter of debate, a clear picture of the structural features of the H-cluster in the $DH_{ox}$ state is presently available. In $DH_{ox}$, the iron atom of the $[2Fe]_H$ subcluster distal relative to the $[4Fe-4S]_H$ cluster ($Fe_d$, see Figure 1; the second iron atom in $[2Fe]_H$ is termed proximal, $Fe_p$) is characterized by a vacant coordination position trans to the $\mu$-CO ligand, where ligands such as $H_2O$ or $H_2$ can be loosely bound.[2,7c,9,18] Indeed, the catalytic cycle for $H_2$ oxidation is thought to imply initial binding of the $H_2$ molecule to the $Fe_d$ atom of the enzyme in the $DH_{ox}$ state, followed by heterolytic cleavage of $H_2$ mediated by the DTMA amine group, and eventually proton and electron release from the enzyme.[18,19]

Prompted by the above observations, we have taken advantage of the wide knowledge on the $DH_{ox}$ redox state to carry out a combined quantum mechanical and molecular mechanics (QM/MM) investigation of the DdH enzyme, in which the electronic properties of all Fe−S clusters in the protein (H-cluster + $Fe_4S_4$ clusters) have been explicitly and simultaneously described using DFT. The main goal of the study was the elucidation of the interplay among the Fe−S clusters in the $DH_{ox}$ redox state of [FeFe]-hydrogenases, as well as the evaluation of the influence of substrate ($H_2$) and ligand ($H_2O$) binding on the electronic and functional properties of the enzyme.

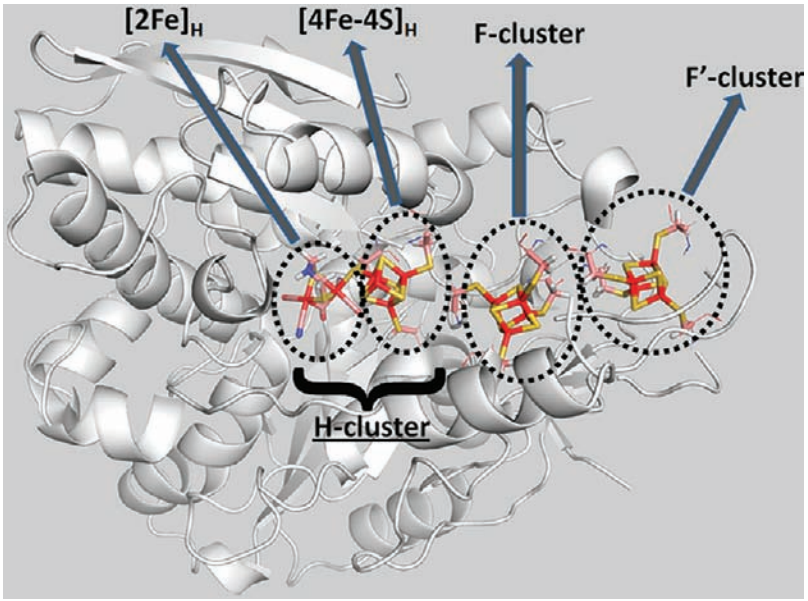


**Figure 2.** Arrangement of Fe−S clusters in the [FeFe]-hydrogenase from *D. desulfuricans* (DdH).

## METHODS

QM/MM approaches based on DFT modeling of the QM region have already proved reliable for the characterization of the electronic properties of large subsystems within proteins.[20] However, the extensive inclusion of Fe−S clusters in the QM region represents a challenge, because these assemblies usually present antiferromagnetic coupling, as in the case of the $[4Fe-4S]_H$, F, and F′ clusters. Such an issue can be tackled by using the broken-symmetry (BS) approach[21] and fast methods for the generation of BS states.[22]

All QM/MM calculations were based on the 1.6-Å resolution structure of DdH (PDB code 1HFE), a heterodimer composed of a small and a large subunit.[1a] In the QM/MM calculations, the protein is divided into two subsystems: System 1 is treated at QM level, and it is allowed to relax. It consists of the atoms in the H, F, and F′ clusters (see below). The remaining portion of the protein, together with the surrounding water molecules, were included in system 2, which is kept fixed at the crystallographic coordinates and is treated at MM level. However, before starting the QM/MM optimization, it is necessary to add the hydrogen atoms that are not detected in the X-ray investigation of the protein. The protonation state of histidine side chains was assigned as previously reported.[18] All Lys and Arg residues were considered in their positively charged state, while Asp and Glu side chains were included in the anionic form. Finally, the iron-bound Cys residues (i.e., amino acids 36, 38, 41, 45, 66, 69, 72, 76, 179, 234, 378, and 382) were assumed to be deprotonated. As a result, the overall charge of the models (full protein, including the inorganic portion, plus solvent) is zero in the case of $\mathbf{DH_{ox}}$, $\mathbf{DH_{ox}}$-$\mathbf{H_2}$, and $\mathbf{DH_{ox}}$-$\mathbf{H_2O}$, whereas it is +2 for $\mathbf{DH_{ox+2}}$, $\mathbf{DH_{ox+2}}$-$\mathbf{H_2O}$, and $\mathbf{DH_{ox\_5CO}}$ (vide infra for details on the composition of the QM region of the models).

After addition of the hydrogen atoms to the crystal structure, the protein was solvated in a sphere of water molecules with a radius of 48 Å with the Amber leap module. In order to optimize the positions of hydrogen atoms and solvent water molecules, a 90 ps simulated annealing molecular dynamics calculation was carried out, followed by 10000 steps of conjugate-gradient energy minimization, keeping all the other atoms fixed at their positions in the crystal structure. All the metal-bound ligands found in the PDB file were included in the QM/MM model, except a water molecule bridging $Fe_d$ and $Fe_p$, which was replaced by a carbonyl group, following a more recent correction to the original crystal structure.[1b]

All the QM/MM optimizations were carried out with the COMQUM program,[23] using TURBOMOLE[24] for the QM part and AMBER 8[25] (with the Amber 1999 force-field)[26] for the MM part. The QM calculations were carried out within the density functional theory (DFT) framework, using the B3LYP functional[27] and an all-electron SVP basis set with polarization functions on all atoms.[28] The use of the SVP basis has been previously validated.[22] B3LYP gives unpaired spins distributions that are in better agreement with EPR and Mössbauer experimental data when compared with results obtained using pure functionals.[29] However, calculations were carried out also at the BP86/SVP level, and the conclusions one can draw from the latter results are compatible with the picture coming from B3LYP/SVP optimizations (see Supporting Information).

The antiferromagnetic coupling that characterizes the $Fe_4S_4$ assemblies included in the QM region of the QM/MM model was treated by means of the BS approach.[21,22] Details on the BS scheme used are given in the Supporting Information.

In the QM calculations, all atoms in system 2 are represented by a partial point charge. These charges are included in the Hamiltonian of the QM calculations, and thus the quantum-chemical system is polarized by the atoms of system 2 in a self-consistent way. When the quantum and classical regions are connected by a chemical bond, the hydrogen link-atom approach is applied,[30] i.e., the QM system is truncated with hydrogen atoms, the positions of which are linearly related to the corresponding carbon atom in the protein. The total QM/MM energy is calculated as:

$$E_{QM/MM} = E_{QM1} + E_{MM12} - E_{MM1} \quad (1)$$

Here, $E_{QM1}$ is the QM energy of the quantum system truncated by hydrogen atoms, including the interaction between system 1 and the surrounding point charges. $E_{MM1}$ is the MM energy of the quantum system, still truncated by hydrogen atoms, but without any electrostatic interactions. Finally, $E_{MM12}$ is the classical energy (including nonbonded interactions between the QM and MM part) of all the atoms in the system with carbon atoms at the junctions and with the charges of the QM region zeroed, to avoid double counting of the electrostatic interactions. Such an approach, which is similar to the one used in the Oniom method,[31] should lead to the cancelation of errors caused by the truncation of the quantum system.

The QM system (system 1) of the various [FeFe]-hydrogenase models always included the iron and sulfide ions of the $Fe_6S_6$ H-cluster and of the $Fe_4S_4$, F, and F′ clusters, the DTMA ligand, three CO groups, two CN ligands (in the all-CO model, these two ligands were replaced by two CO ligands), and twelve $CH_3S$ fragments that represent the Cys residues connecting the H, F, and F′ clusters to the rest of the enzyme large subunit. Some of the models included also an additional $H_2$ or $H_2O$ ligand, as specified in Results and Discussion. The total number of atoms in the QM system thus varies between 106 and 109.

We have also carried out multiple 10 ns molecular dynamics simulations to test the structural stability of the models used in QM/MM calculations and to verify that the changes in the electronic structures of the Fe−S clusters do not affect significantly the conformation of the surrounding residues. Details about these calculations are reported in the Supporting Information.

## RESULTS AND DISCUSSION

**Characterization of the Electronic Structure of the Active-Ready $DH_{ox}$ Enzyme State.** A fundamental premise for the investigation of the effects of ligand binding on the electronic properties of the Fe−S clusters of [FeFe]-hydrogenases is the reliable assignment of the H-cluster redox state in the $DH_{ox}$ state. As mentioned in the Introduction, the EPR data[14] available for the $DH_{ox}$ enzyme form indicate that both the $[4Fe-4S]_H$ subcluster and the F and F′ clusters are in the diamagnetic 2Fe(II)2Fe(III) state. As for the $[2Fe]_H$ subsite, comparisons between experimental and computed vibrational frequencies, as well as EPR parameters, indicate a Fe(I)Fe(II) state.[17,32] This picture is supported also by complementary data collected studying biomimetic organometallic compounds[33] and small-size QM models of either the whole H-cluster[34] or its binuclear subsite.[17,35] However, as recently noticed by Lubitz et al.,[9] Mössbauer data on $DH_{ox}$ are also compatible with a $[2Fe]_H$ subsite attaining the Fe(II)Fe(III) redox state. Moreover, in a recent QM/MM study, it was suggested that a catalytic cycle involving Fe(II)Fe(III) species has a reasonable energy profile.[36] Therefore, we have initially used our QM/MM model of the *Desulfovibrio* enzyme to evaluate if the Fe(II)Fe(III) and Fe(II)Fe(I) redox states of the $[2Fe]_H$ subsite are compatible with the simultaneous presence in $DH_{ox}$ of diamagnetic $[4Fe-4S]_H$, F, and F′ clusters featuring the 2Fe(II)2Fe(III) redox state. In particular, we have first carried out QM/MM geometry optimization of an enzyme form ($\mathbf{DH_{ox+2}}$) characterized by a −5 total charge of the QM subsystem (see Methods for details), which formally corresponds to a Fe(II)Fe(III) redox state of the $[2Fe]_H$ subcluster and a 2Fe(II)2Fe(III) redox state of the $[4Fe-4S]_H$, F, and F′ clusters, respectively (here and in the following we formally assign the charge and spin of the bridging Cys ligand to the $[4Fe-4S]_H$ subcluster).

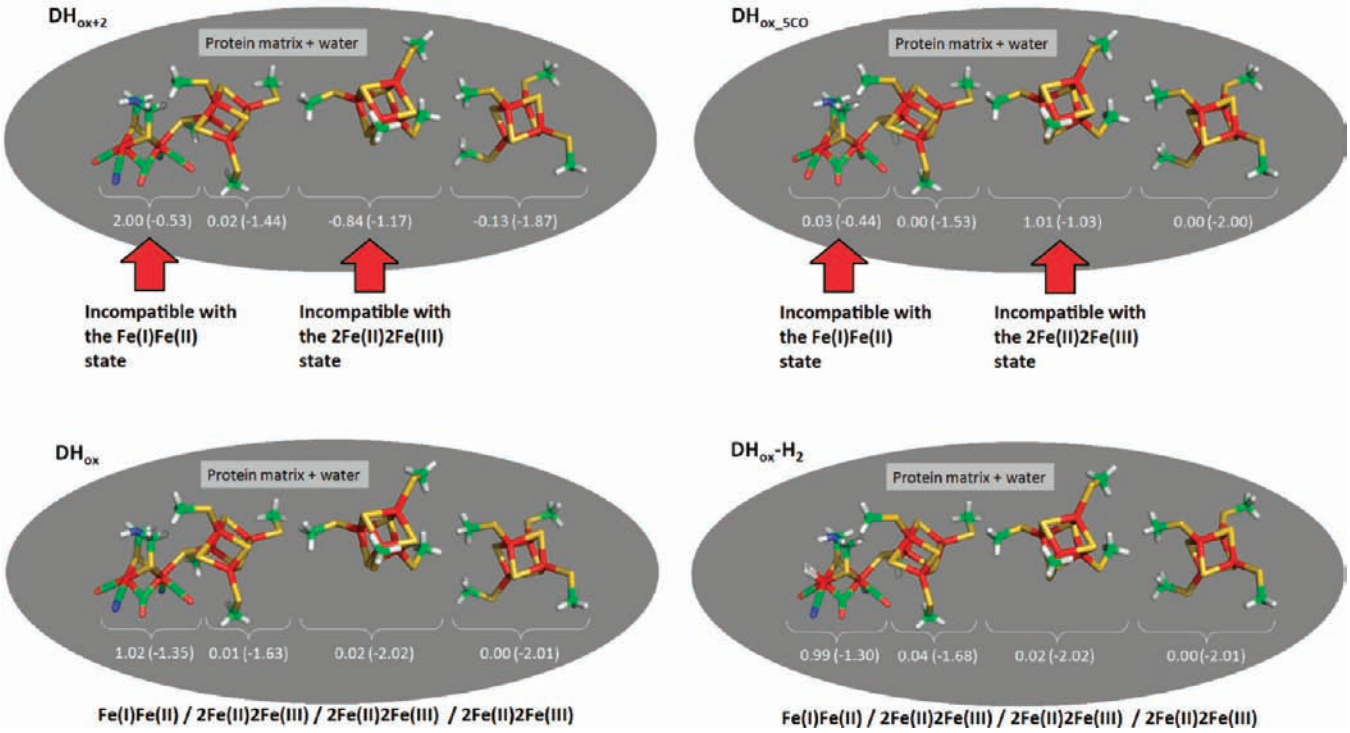


**Figure 3.** Geometries, spin populations, charges (in brackets), and formal oxidation states of the Fe−S clusters in the QM/MM models **DH$_{ox+2}$**, **DH$_{ox}$**, **DH$_{ox}$-H$_2$**, and **DH$_{ox_5CO}$**. The following atom colors are used: red for Fe, yellow for S, white for H, blue for N, green for C, and light red for O. The Fe$_d$−Fe$_p$ and Fe$_p$−S(Cys) bond lengths as well as the average bond lengths between the iron ions and the cysteine sulfur atoms in the [4Fe−4S]$_H$, F, and F′-clusters are as follows: 2.68, 2.44, 2.31, 2.28, 2.30 Å in **DH$_{ox+2}$**, 2.55, 2.44, 2.31, 2.33, 2.31 Å in **DH$_{ox}$**, 2.65, 2.52, 2.31, 2.33, 2.31 Å in **DH$_{ox}$-H$_2$**, and 2.62, 2.44, 2.31, 2.26, 2.31 Å in **DH$_{ox_5CO}$**, respectively.

The QM/MM results clearly show that the Fe(II)Fe(III) state of the [2Fe]$_H$ subsite is not compatible with the presence of [4Fe-4S]$_H$, F, and F′ clusters in the 2Fe(II)2Fe(III) redox state. In fact, in the optimized **DH$_{ox+2}$** model (Figure 3) the [2Fe]$_H$ subcluster features a total charge as low as −0.5, i.e., approximately 1.5 *e* more negative than the +1 formal charge corresponding to the Fe(II)Fe(III) state. In addition, the F-cluster reaches a charge and spin population of −1.2 and −0.8, respectively, indicating formation of an oxidized Fe(II)3Fe(III) state instead of the experimentally observed 2Fe(II)2Fe(III) state. Therefore, the analysis of the electronic structure of **DH$_{ox+2}$** indicates that the [2Fe]$_H$ subcluster posed at the Fe(II)Fe(III) redox state would spontaneously evolve toward a Fe(II)Fe(II) state, with concomitant oxidation of the F-cluster.

Addition of two electrons to the **DH$_{ox+2}$** model results in a species (**DH$_{ox}$**) that, after optimization, is characterized by zero spin population at the [4Fe-4S]$_H$, F, and F′ clusters (Figure 3), as expected for diamagnetic $Fe_4S_4$ clusters, while the unpaired electron is localized on the [2Fe]$_H$ subcluster, in agreement with EPR and Mössbauer results for the DH$_{ox}$ state.[14,15] Moreover, the F and F′ clusters have Mulliken charges close to the formal −2 charge expected for a 2Fe(II)2Fe(III) state. In addition, the overall charge of the H-cluster (−3.0) is compatible with a Fe(I)Fe(II)−2Fe(II)2Fe(III) redox state. Therefore, we can confidently conclude that in the DH$_{ox}$ state, the [2Fe]$_H$ subcluster is characterized by the Fe(I)Fe(II) redox state. Similar results are obtained by calculations carried out on **DH$_{ox}$** and **DH$_{ox+2}$** variants featuring a water molecule weakly bound to Fe$_d$ (models **DH$_{ox+2}$-H$_2$O** and **DH$_{ox}$-H$_2$O**; see Supporting Information).

**Role of CN Ligands on the Redox Properties of DH$_{ox}$.** A key issue in hydrogenases chemistry is the role played by the biologically unusual cyanide ligands. We have recently reported that the cyanide ligands are crucial for the proper redox interplay between the two subclusters that compose the H-cluster. In fact, we showed that the substitution of both CN ligands with carbonyls would impair the ability of the [2Fe]$_H$ cluster to reach the Fe(I)Fe(II) redox state upon one-electron oxidation of the reduced H-cluster, a fact that is expected to lower the electrophilicity of the enzyme active site and its affinity toward $H_2$.[37] These previous observations prompted us to study the role of cyanide ligands on the electronic properties of the whole chain of Fe−S clusters in DdH. To this end, we substituted the two CN ligands in the **DH$_{ox}$** model with CO groups, obtaining the model **DH$_{ox_5CO}$** (see Figure 3). After QM/MM geometry optimization, the electronic structure analysis showed that CN/CO substitution has a large impact not only on the H-cluster electronic structure, as previously noted, but also on the other Fe−S clusters. In fact, in **DH$_{ox_5CO}$** the [2Fe]$_H$ subcluster switches from the paramagnetic Fe(I)Fe(II) state to a diamagnetic state, as deduced by comparison of the [2Fe]$_H$ spin populations in **DH$_{ox}$** and in **DH$_{ox_5CO}$** (1.0 and 0.0, respectively; see Figure 3). Moreover, the overall charge of the H-cluster in **DH$_{ox_5CO}$** (−2.0, Figure 3) is compatible with a formal Fe(I)Fe(I)−2Fe(II)2Fe(III) redox state. This means that the [2Fe]$_H$ subcluster reaches a lower oxidation state in **DH$_{ox_5CO}$**, when compared to the **DH$_{ox}$** model. Concomitantly, the F-cluster is oxidized and reaches the paramagnetic Fe(II)3Fe(III) state in **DH$_{ox_5CO}$** (Mulliken charge and spin population = −1.0 and 1.0, respectively).


dx.doi.org/10.1021/ja205542k |*J. Am. Chem. Soc.* 2011, 133, 18742–18749

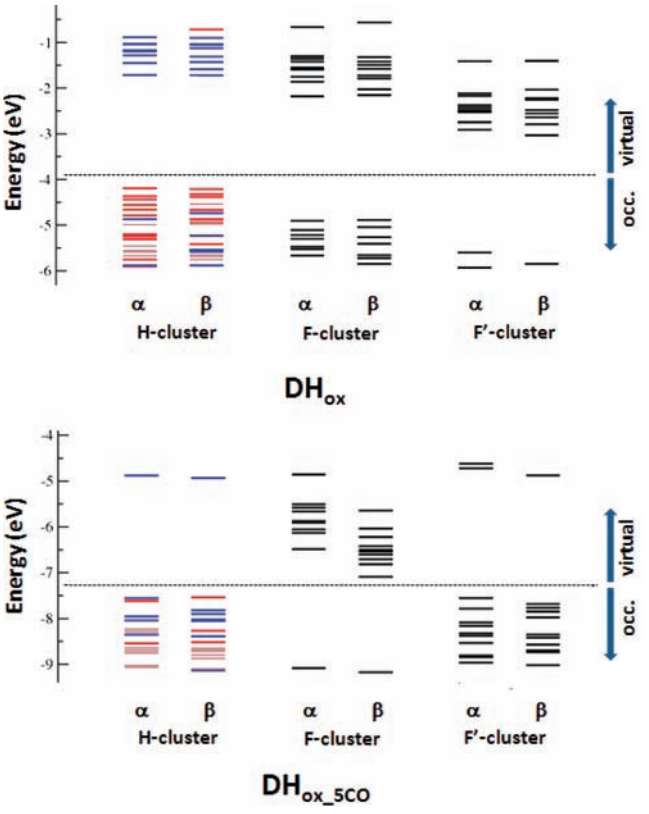


**Figure 4.** Detailed orbital diagrams of models $\mathbf{DH_{ox}}$ and $\mathbf{DH_{ox\_5CO}}$. The dotted horizontal line marks the separation between occupied and unoccupied orbitals. MOs localized on the H-cluster are distinguished by the use of different colors (red, blue, or gray for orbitals centered on the $[2Fe]_H$ subcluster, on the $[4Fe\text{-}4S]_H$ subcluster, or delocalized over these two subclusters, respectively).

A comparison between energy diagrams of molecular orbitals in $\mathbf{DH_{ox}}$ and $\mathbf{DH_{ox\_5CO}}$ visualizes further key details of the effects of CN/CO substitutions on the electronic properties of the enzyme. In fact, Figure 4 shows that the highest occupied molecular orbitals (HOMOs) in $\mathbf{DH_{ox}}$ are localized on the H-cluster, while the occupied MOs centered on the F′-cluster are found at energy values that are at least 1.3 eV lower than the HOMO energy level. Conversely, in $\mathbf{DH_{ox\_5CO}}$ the HOMOs are localized not only on the H-cluster but also on the F′-cluster, whereas the MOs localized on the F-cluster are shifted to relatively lower energies. The latter is a result of the above-mentioned one-electron oxidation of the F-cluster upon CN/CO substitutions in the H-cluster. Finally, also the distribution of unoccupied MOs in the two energy diagrams of Figure 4 is significantly different. Most notably, the lowest unoccupied molecular orbital (LUMO) is localized on the F′-cluster in $\mathbf{DH_{ox}}$, whereas it is centered on the F-cluster in $\mathbf{DH_{ox\_5CO}}$.

**Effects of Substrate ($H_2$) and Ligand ($H_2O$) Binding on the Electronic Properties of the $DH_{ox}$ Redox Form of the Enzyme.** As mentioned above, the partially oxidized $DH_{ox}$ form of the enzyme is involved in $H_2$ binding.[9,34,35] In particular, in [FeFe]-hydrogenases that are physiologically involved in $H_2$ uptake, binding of $H_2$ to the $[2Fe]_H$ subcluster was proposed to be immediately followed by $H_2$ oxidation and concomitant F-cluster reduction (e.g., in CpII). This picture, originally proposed by Adams,[10] is supported by the experimental observation that the F-clusters in CpII feature redox potentials between −180 and −300 mV, much less negative than that of the H-cluster (−410 mV). On the contrary, in the CpI hydrogenase, which is "reversible", meaning that it is able to efficiently catalyze both the reduction of protons and $H_2$ oxidation, the redox potentials of the H-cluster and of the ancillary clusters are very close to each other,[10] such that electrons can be easily mobilized both toward and from the active site. Adams proposed that in the case of $H_2$ binding to reversible hydrogenases, there is no immediate oxidation of $H_2$ with concomitant reduction of one of the F-clusters, because of the relatively low redox potential of the latter.[10] In view of these observations, we have investigated the effects of $H_2$ binding to $Fe_d$ on the electronic structure of the DdH, which is a reversible hydrogenase as well. To this end, a model in which a $H_2$ molecule is coordinated to the $Fe_d$ atom of the $DH_{ox}$ form ($\mathbf{DH_{ox}\text{-}H_2}$) was optimized and analyzed.

Comparison of Mulliken charges and spin populations in $\mathbf{DH_{ox}\text{-}H_2}$ and $\mathbf{DH_{ox}}$ (Figure 3) suggests that the redox state of the Fe−S clusters is not affected by $H_2$ binding. However, fine modifications of the electronic structure of the enzyme upon $H_2$ binding are evident and can be highlighted by comparing molecular orbitals of the $\mathbf{DH_{ox}\text{-}H_2}$ and $\mathbf{DH_{ox}}$ models (Figures 4 and 5).

In the case of $\mathbf{DH_{ox}}$, the unoccupied MOs localized on the F′-cluster are among the lowest-lying virtual orbitals: They are found approximately 1.2 eV above the HOMO level; see Figure 4. Such a feature is functional for a facile reduction of the F′-cluster, which is the most solvent-exposed Fe−S site, thus prone to interactions with the physiological redox partners of the enzyme.

As far as $H_2$ binding is concerned, it is worth noting that $\mathbf{DH_{ox}}$ features a low-lying virtual orbital localized on the H-cluster binuclear subsite (Figure 4). As mentioned in a previous work,[34] an MO with these characteristics is ready to interact with the electron density of the H−H bond in $H_2$, thus explaining the electrophilic behavior of $\mathbf{DH_{ox}}$ and the ability of this enzyme state to bind $H_2$. Accordingly, it is not surprising to find that the HOMO of the $H_2$-bound adduct $\mathbf{DH_{ox}\text{-}H_2}$ is localized on the enzyme active site (see the MOs energy ranking of the latter model, reported in Figure 5).

The LUMO in $\mathbf{DH_{ox}\text{-}H_2}$ is localized on the F′-cluster, not differently from the case of $\mathbf{DH_{ox}}$. However, the HOMO−LUMO gap is significantly smaller in $\mathbf{DH_{ox}\text{-}H_2}$ than in $\mathbf{DH_{ox}}$: 0.6 vs 1.2 eV, respectively (see Figures 4 and 5). Such shrinking of the energy gap, which is induced by $H_2$ binding, suggests that the F′-cluster might withdraw one electron from the H-cluster when an exogenous polarizing species is bound to the enzyme.

In this context, it is worth emphasizing that in the $H_2$ oxidation reaction catalyzed by [FeFe]-hydrogenases, $H_2$ is not the only substrate of the enzyme, because during catalysis electrons are transferred from the enzyme to physiological redox partners,[10] such as cytochrome $c_{553}$.[38] Binding of such physiological redox partners is expected to affect the electronic structure of [FeFe]-hydrogenases, withdrawing electron density from the active site and possibly triggering $[2Fe]_H$ subcluster oxidation and $H_2$ activation. In fact, it was shown that heterolytic $H_2$ cleavage takes place only when the $[2Fe]_H$ subcluster is in the Fe(II)Fe(II) redox state (i.e., a state which is one electron more oxidized than in the resting $DH_{ox}$ form).[18] Unfortunately, the computational study of intermolecular electron transfer is currently problematic because of the large size of the protein−protein complex and also because no crystal structure of the DdH−cytochrome $c_{553}$ complex is available.[39] However, to test the hypothesis that the redox potential of the $[2Fe]_H$ subcluster would change upon $H_2$ binding,

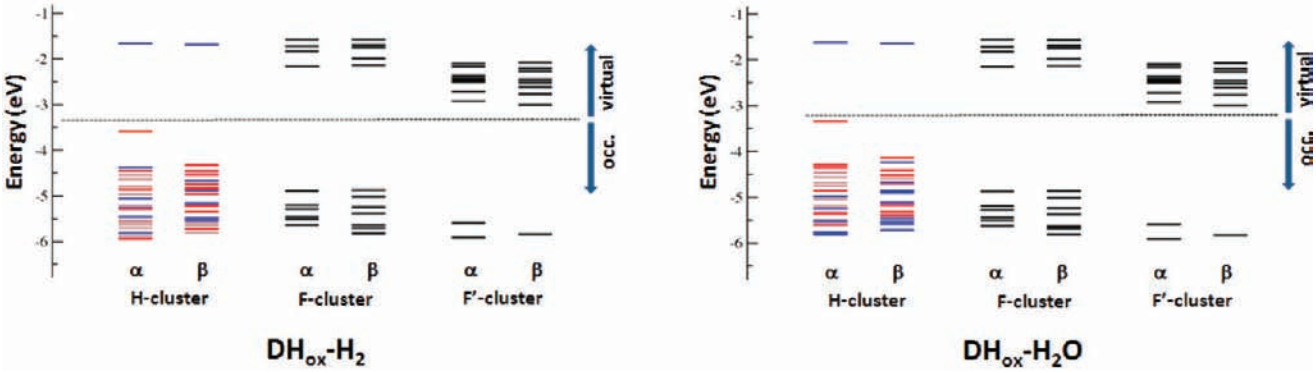


**Figure 5.** Detailed orbital diagram of models $\mathbf{DH_{ox}}$-$\mathbf{H_2}$ and $\mathbf{DH_{ox}}$-$\mathbf{H_2O}$. The dotted horizontal line marks the separation between occupied and unoccupied orbitals. MOs localized on the H-cluster are distinguished by the use of different colors (red, blue, or gray for orbitals centered on the $[2Fe]_H$ subcluster, on the $[4Fe\text{-}4S]_H$ subcluster, or delocalized over these two subclusters, respectively).

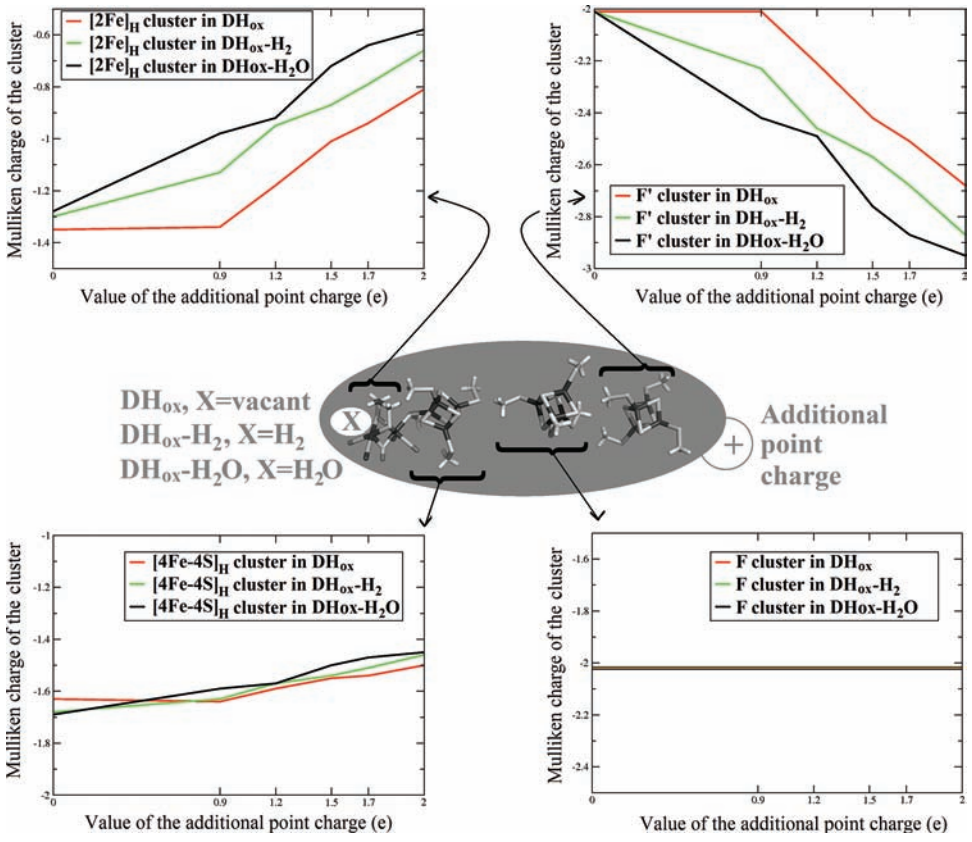


**Figure 6.** Variation of Mulliken charges of the $[2Fe]_H$, $[4Fe\text{-}4S]_H$, F, and F′ clusters in models $\mathbf{DH_{ox}}$, $\mathbf{DH_{ox}}$-$\mathbf{H_2}$, and $\mathbf{DH_{ox}}$-$\mathbf{H_2O}$, as a function of the increasing value of the additional point charge with which such models were supplemented.

we have carried out a new set of QM/MM calculations in which the polarization effects due to the binding of redox partners to [FeFe]-hydrogenases was *qualitatively* evaluated by the introduction of electron-withdrawing probes, such as cationic species, in the MM region of the QM/MM models.

In particular, single-point SCF calculations on $\mathbf{DH_{ox}}$ and $\mathbf{DH_{ox}}$-$\mathbf{H_2}$ models have been carried out after replacement of the solvent water molecule closest to the F′-cluster with a probe characterized by an increasing positive charge (0.9, 1.2, 1.5, 1.7, 2 au, respectively). The effect of the cationic probe on the overall charge of the $[2Fe]_H$ and F′ clusters is shown in Figure 6. It turned out that the polarizing effect of the cationic probe promotes electron transfer from the $[2Fe]_H$ subcluster to the F′ cluster, while the overall charge of the $[4Fe\text{-}4S]_H$ and F cluster remains essentially unaffected (Figure 6). More importantly, oxidation of the $[2Fe]_H$ subcluster and concomitant reduction of the F′ cluster is more favored in $\mathbf{DH_{ox}}$-$\mathbf{H_2}$ than in $\mathbf{DH_{ox}}$. This effect is functionally relevant, because it indicates that if a suitable polarizing or redox partner is bound in proximity of the F′-cluster, oxidation of the $[2Fe]_H$ cluster can be triggered by substrate binding.


dx.doi.org/10.1021/ja205542k |*J. Am. Chem. Soc.* 2011, 133, 18742–18749

**Scheme 1. Schematic Representation of the Reactivity of $DH_{ox}$ with $H_2$, $H_2O$, and a Generic Redox Partner (indicated as RP)[a]**

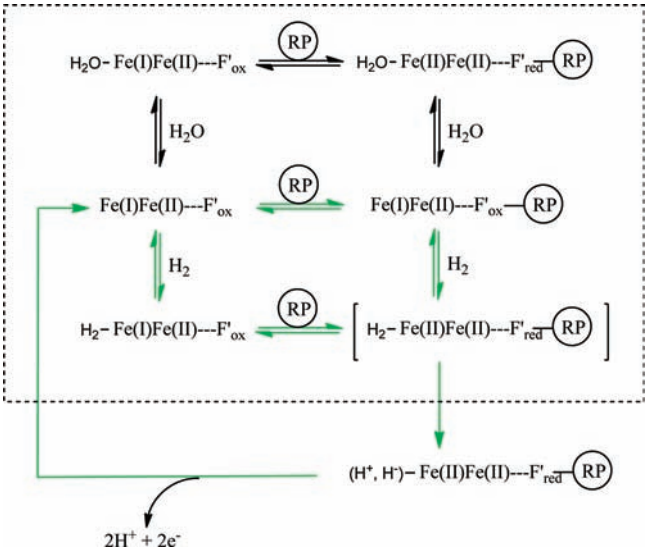


[a] The oxidized 2Fe(II)2Fe(III) and reduced 3Fe(II)Fe(III) states of the F′-cluster are schematically indicated using the labels $F'_{ox}$ and $F'_{red}$, respectively. The enzyme forms discussed in this work are inside the dotted box. Reaction steps that are relevant in the catalytic cycle leading to $H_2$ oxidation are colored in green.

As mentioned in the Introduction, a water molecule could be loosely bound to the distal iron atom in the $DH_{ox}$ redox state of the enzyme. This observation prompted us to evaluate how the binding of a $H_2O$ molecule to the H-cluster ($\mathbf{DH_{ox}\text{-}H_2O}$) affects the electronic structure of the Fe−S clusters, using as reference the electronic structure of the $\mathbf{DH_{ox}\text{-}H_2}$ adduct. Notably, a schematic representation of molecular orbitals reveals that the electronic structures of $\mathbf{DH_{ox}\text{-}H_2O}$ and $\mathbf{DH_{ox}\text{-}H_2}$ are extremely similar (Figure 5; see also the Supporting Information for clusters charges and spin densities in $\mathbf{DH_{ox}\text{-}H_2O}$). Therefore, according to our QM/MM calculations, binding of a water molecule could also facilitate electron transfer from the $[2Fe]_H$ subcluster to the F′-cluster, if a suitable polarizing molecule is bound close to the F′-cluster. However, binding of a $H_2$ molecule followed by one-electron oxidation of the Fe(I)Fe(II) $[2Fe]_H$ cluster increases the acidity of the metal-bound $H_2$ molecule to such an extent to trigger its heterolytic cleavage,[18] which eventually leads to release of two protons and two electrons from the enzyme, whereas $H_2O$ binding leads to a dead-end reaction pathway that can be best described as a simple equilibrium between a Fe(II)Fe(I)−$F'_{ox}$ and a $H_2O$−Fe(II)Fe(II)−$F'_{red}$ species (Scheme 1). In this context, it is noteworthy that purified preparations of DdH at pH < 6 are inactivated in protein-film voltammetry experiments conducted at potentials higher than 0.05 V.[11] Such inactivation was proposed to originate from a one-electron oxidation of $DH_{ox}$,[11] that would lead to a water-bound, inhibited $[2Fe]_H$ cluster attaining the Fe(II)Fe(II) state. The resulting $H_2O$−Fe(II)Fe(II) species is expected to easily reactivate upon one-electron reduction,[11] thus defining an equilibrium analogous to the one described above for the enzyme−cytochrome complex.

## CONCLUSIONS

By using DFT in the context of a QM/MM, broken-symmetry representation of the [FeFe]-hydrogenase from *D. desulfuricans*, we have characterized fundamental properties of the enzymatic Fe−S cluster chain. The approach applied here is based on the inclusion of the whole inorganic subsystem (H-cluster, F, and F′ clusters) in the quantum-mechanical portion of the model. As a first step, we used such a model to show that the partially oxidized, active-ready form of DdH cannot attain the Fe(II)Fe(III) redox state at the catalytic $[2Fe]_H$ subsite. In fact, even though the Fe(II)Fe(III) state is compatible with previous Mössbauer results,[6,9] it turned out to be at odds with the actual relative redox potentials of the Fe−S assemblies in the enzyme. On the other hand, full consistency between theory and experiments is observed in the case of the alternative Fe(I)Fe(II) redox state.

Our QM/MM results confirm and extend previous findings,[37] indicating that the natural selection of biologically unusual CN ligands has a profound effect in terms of balancing the redox properties of the various clusters in the [FeFe]-hydrogenases. In fact, the replacement of the naturally occurring CN ligands with carbonyl groups would give way to a dramatic modification of DdH electronic structure.

We have also investigated the electronic effects of $H_2$ (substrate) binding to the H-cluster. It turned out that even though $H_2$ binding to the active-ready enzyme does not significantly influence the charges and spin populations of the clusters, it clearly leads to a decrease of the HOMO−LUMO gap. Such a reorganization of the electronic structure is relevant from a functional point of view, because the HOMO is localized on the H-cluster, while the LUMO is centered on the solvent-exposed F′-cluster. Therefore, a reduction of the gap between such molecular orbitals is expected to favor long-range electron transfer within the protein matrix. Actually, electron transfer from the H-cluster to the F′-cluster turned out to be favored in the $H_2$-bound form of $DH_{ox}$, when the polarizing effects of [FeFe]-hydrogenases redox partners are modeled by means of a simple point-charge representation. These results show the intimate connection between the electronic structure of the whole enzyme and its ability to establish a fruitful interplay with exogenous cellular redox partners of physiological importance. Such a biochemical issue has relevant bearings also on the quest for biomimetic reproduction of the enzyme function in organometallic compounds: In fact, in a recent contribution it was shown that proton-coupled electron transfer involving mild oxidants can play a key role in the $H_2$ oxidation catalyzed by synthetic models of [FeFe]-hydrogenases.[40]

DdH is a "reversible" enzyme, meaning that it is able to efficiently catalyze the reaction $H_2 \leftrightarrows 2H^+ + 2e^-$ in both directions.[10,11,41] Our results support the hypothesis that this reversibility depends on the possibility to easily modulate the cluster redox potentials,[10] to mobilize electrons along any of the two possible directions, i.e., toward the catalytically active H-cluster during $H_2$ evolution or toward the protein surface during $H_2$ oxidation, depending on the cellular metabolic state. Moreover, our findings let us envisage future perspectives for a targeted introduction of mutations in the enzyme, to change its specificity. In the case of DdH in particular, the introduction of positively charged residues (arginine or lysine moieties) spatially close to the F′-cluster might lead to polarization effects similar to those induced in our models by the charge probes used to simply mimic

the binding of a physiologically relevant redox partner. This might transform the reversible DdH enzyme into a monodirectional mutant featuring enhanced $H_2$-oxidizing properties.

Finally, the theoretical approach presented here, i.e., studying a metalloenzyme by including its whole inorganic, redox-active portion in the high-level DFT treatment, may allow the characterization of some aspects of electron-transfer events of functional importance also in other classes of oxidoreductases featuring multiple Fe−S clusters.

## ■ ASSOCIATED CONTENT

**Supporting Information.** Discussion of the BS coupling scheme used for the models described in the paper; results of single-point B3LYP calculations carried out in a vacuum on the QM systems extracted from the optimized QM/MM models, and corresponding geometrical coordinates and energies; details on results obtained using an alternative BS coupling scheme as well as an alternative functional (BP86); methodological details and results of MD simulations on selected enzyme models; complete list of authors for reference 25. This material is available free of charge via the Internet at http://pubs.acs.org.

## ■ AUTHOR INFORMATION

**Corresponding Author**
grecocla@hu-berlin.de; luca.degioia@unimib.it

## ■ ACKNOWLEDGMENT

C.G. gratefully acknowledges CINECA (Bologna, Italy) for having provided high-performance computational resources. C.G. also acknowledges support from the Cluster of Excellence "Unifying concepts in catalysis" (UNICAT), coordinated by the Technische Universität Berlin.

## ■ REFERENCES

(1) (a) Nicolet, Y.; Piras, C.; Legrand, P.; Hatchikian, C. E.; Fontecilla-Camps, J. C. *Struct. Fold. Des.* **1999**, *7*, 13. (b) Nicolet, Y.; de Lacey, A. L.; Vernede, X.; Fernandez, V. M.; Hatchikian, E. C.; Fontecilla-Camps, J. C. *J. Am. Chem. Soc.* **2001**, *123*, 1596. (c) Peters, J. W.; Lanzilotta, W. N.; Lemon, B. J.; Seefeldt, L. C. *Science* **1998**, *282*, 1853. (d) Pandey, A. S.; Harris, T. V.; Giles, L. J.; Peters, J. W.; Szilagyi, R. K. *J. Am. Chem. Soc.* **2008**, *130*, 4533.

(2) Lemon, B. J.; Peters, J. W. *Biochemistry* **1999**, *38*, 12969.

(3) (a) Silakov, A.; Wenk, B.; Reijerse, E.; Lubitz, W. *Phys. Chem. Chem. Phys.* **2009**, *11*, 6592. (b) Erdem, O. F.; Schwartz, L.; Stein, M.; Silakov, A.; Kaur-Ghumaan, S.; Huang, P.; Ott, S.; Reijerse, E. J.; Lubitz, W. *Angew. Chem., Int. Ed.* **2011**, *50*, 1439.

(4) Pilet, E.; Nicolet, Y.; Mathevon, C.; Douki, T.; Fontecilla-Camps, J. C.; Fontecave, M. *FEBS Lett.* **2009**, *583*, 506.

(5) Ryde, U.; Greco, C.; De Gioia, L. *J. Am. Chem. Soc.* **2010**, *132*, 4512.

(6) Popescu, C. V.; Munck, E. *J. Am. Chem. Soc.* **1999**, *121*, 7877.

(7) (a) Hatchikian, E. C.; Forget, N.; Fernandez, V. M.; Williams, R.; Cammack, R. *Eur. J. Biochem.* **1992**, *209*, 357. (b) Pierik, A. J.; Hagen, W. R.; Redeker, J. S.; Wolbert, R. B. G.; Boersma, M.; Verhagen, M.; Grande, H. J.; Veeger, C.; Mutsaers, P. H. A.; Sands, R. H.; Dunham, W. R. *Eur. J. Biochem.* **1992**, *209*, 63. (c) Albracht, S. P. J.; Roseboom, W.; Hatchikian, E. C. *J. Biol. Inorg. Chem.* **2006**, *11*, 88.

(8) Wang, G.; Benecky, M. J.; Huynh, B. H.; Cline, J. F.; Adams, M. W.; Mortenson, L. E.; Hoffman, B. M.; Münck, E. *J. Biol. Chem.* **1984**, *259*, 14328.

(9) Lubitz, W.; Reijerse, E.; van Gastel, M. *Chem. Rev.* **2007**, *107*, 4331.

(10) Adams, M. W. W. *Biochim. Biophys. Acta* **1990**, *1020*, 115.

(11) Parkin, A.; Cavazza, C.; Fontecilla-Camps, J. C.; Armstrong, F. A. *J. Am. Chem. Soc.* **2006**, *128*, 16808.

(12) Voordouw, G.; Brenner, S. *Eur. J. Biochem.* **1985**, *148*, 515.

(13) Hatchikian, E. C.; Magro, V.; Forget, N.; Nicolet, Y.; Fontecilla-Camps, J. C. *J. Bacteriol.* **1999**, *181*, 2947.

(14) Patil, D. S.; Moura, J. J. G.; He, S. H.; Teixeira, M.; Prickril, B. C.; Dervartanian, D. V.; Peck, H. D.; Legall, J.; Huynh, B. H. *J. Biol. Chem.* **1988**, *263*, 18732.

(15) Pereira, A. S.; Tavares, P.; Moura, I.; Moura, J. J. G.; Huynh, B. H. *J. Am. Chem. Soc.* **2001**, *123*, 2771.

(16) Roseboom, W.; De Lacey, A. L.; Fernandez, V. M.; Hatchikian, E. C.; Albracht, S. P. J. *J. Biol. Inorg. Chem.* **2006**, *11*, 102.

(17) Tye, J. W.; Darensbourg, M. Y.; Hall, M. B. *Inorg. Chem.* **2008**, *47*, 2380. Yu, L.; Greco, C.; Bruschi, M.; Ryde, U.; De Gioia, L.; Reiher, M. *Inorg. Chem.* **2011**, *50*, 3888.

(18) Greco, C.; Bruschi, M.; De Gioia, L.; Ryde, U. *Inorg. Chem.* **2007**, *46*, 5911.

(19) Fan, H. J.; Hall, M. B. *J. Am. Chem. Soc.* **2001**, *123*, 3828. Siegbahn, P. E. M.; Tye, J. W.; Hall, M. B. *Chem. Rev.* **2007**, *107*, 4414.

(20) Guallar, V.; Wallrapp, F. *J. R. Soc., Interface* **2008**, *5*, S233.

(21) Noodleman, L.; Norman, J. G. *J. Chem. Phys.* **1979**, *70*, 4903. Noodleman, L. *J. Chem. Phys.* **1981**, *74*, 5737.

(22) Greco, C.; Fantucci, P.; Ryde, U.; De Gioia, L. *Int. J. Quantum Chem.* **2011**, *111*, 3949.

(23) Ryde, U. *J. Comput.-Aided Mol. Des.* **1996**, *10*, 153. Ryde, U.; Olsson, M. H. M. *Int. J. Quantum Chem.* **2001**, *81*, 335.

(24) Ahlrichs, R.; Bar, M.; Haser, M.; Horn, H.; Kolmel, C. *Chem. Phys. Lett.* **1989**, *162*, 165.

(25) Case, D. A. et al. *Amber 8*; University of California, San Francisco, CA, 2004.

(26) Cornell, W. D.; Cieplak, P.; Bayly, C. I.; Gould, I. R.; Merz, K. M.; Ferguson, D. M.; Spellmeyer, D. C.; Fox, T.; Caldwell, J. W.; Kollman, P. A. *J. Am. Chem. Soc.* **1995**, *117*, 5179.

(27) Becke, A. D. *J. Chem. Phys.* **1993**, *98*, 5648. Lee, C. T.; Yang, W. T.; Parr, R. G. *Phys. Rev. B* **1988**, *37*, 785.

(28) Schafer, A.; Horn, H.; Ahlrichs, R. *J. Chem. Phys.* **1992**, *97*, 2571.

(29) Matito, E.; Sola, M. *Coord. Chem. Rev.* **2009**, *253*, 647.

(30) Reuter, N.; Dejaegere, A.; Maigret, B.; Karplus, M. *J. Phys. Chem. A* **2000**, *104*, 1720.

(31) Svensson, M.; Humbel, S.; Froese, R. D. J.; Matsubara, T.; Sieber, S.; Morokuma, K. *J. Phys. Chem.* **1996**, *100*, 19357–19363.

(32) Fiedler, A. T.; Brunold, T. C. *Inorg. Chem.* **2005**, *44*, 9322.

(33) Lyon, E. J.; Georgakaki, I. P.; Reibenspies, J. H.; Darensbourg, M. Y. *Angew. Chem., Int. Ed.* **1999**, *38*, 3178. Le Cloirec, A.; Best, S. P.; Borg, S.; Davies, S. C.; Evans, D. J.; Hughes, D. L.; Pickett, C. J. *Chem. Commun.* **1999**, 2285. Schmidt, M.; Contakes, S. M.; Rauchfuss, T. B. *J. Am. Chem. Soc.* **1999**, *121*, 9736.

(34) Bruschi, M.; Greco, C.; Fantucci, P.; De Gioia, L. *Inorg. Chem.* **2008**, *47*, 6056.

(35) Cao, Z. X.; Hall, M. B. *J. Am. Chem. Soc.* **2001**, *123*, 3734.

(36) Trohalaki, S.; Pachter, R. *Int. J. Hydrogen Energy* **2010**, *35*, 5318.

(37) Bruschi, M.; Greco, C.; Bertini, L.; Fantucci, P.; Ryde, U.; De Gioia, L. *J. Am. Chem. Soc.* **2010**, *132*, 4992.

(38) Verhagen, M. F.; Wolbert, R. B.; Hagen, W. R. *Eur. J. Biochem.* **1994**, *221*, 821.

(39) Morelli, X.; Czjzek, M.; Hatchikian, C. E.; Bornet, O.; Fontecilla-Camps, J. C.; Palma, N. P.; Moura, J. J.; Guerlesquin, F. *J. Biol. Chem.* **2000**, *275*, 23204.

(40) Camara, J. M.; Rauchfuss, T. B. *J. Am. Chem. Soc.* **2011**, *133*, 8098.

(41) Frey, M. *ChemBioChem* **2002**, *3*, 153.